Article

Cell Systems

In Vivo Decoding Mechanisms of the Temporal Patterns of Blood Insulin by the Insulin-AKT Pathway in the Liver

Graphical Abstract

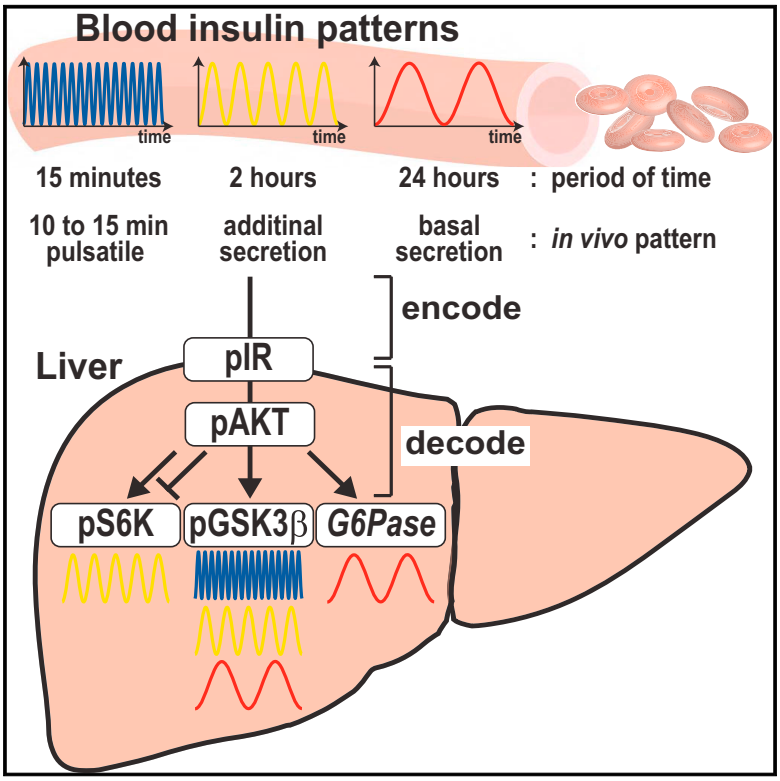

Highlights

- Insulin selectively regulates signaling molecules via temporal patterns *in vivo*
- We measured signaling activities in the liver by a hyperinsulinemic-euglycemic clamp
- Mathematical modeling revealed the temporal coding mechanism of insulin actions
- Insulin patterns, encoded in the IR, are selectively decoded by downstream molecules

Authors

Hiroyuki Kubota, Shinsuke Uda, Fumiko Matsuzaki, Yukiyo Yamauchi, Shinya Kuroda

Correspondence

kubota@bioreg.kyushu-u.ac.jp (H.K.), skuroda@bs.s.u-tokyo.ac.jp (S.K.)

In Brief

Kubota et al. show that the insulin-AKT pathway in the liver processes the information encoded into the temporal patterns of blood insulin and selectively regulates downstream molecules. Given that almost all hormones exhibit distinct temporal patterns, our study demonstrates the possibility of temporal coding as a general principle of systemic homeostasis by hormones.

Kubota et al., 2018, Cell Systems *7*, 1–11
July 25, 2018
https://doi.org/10.1016/j.cels.2018.05.013

CellPress

Please cite this article in press as: Kubota et al., *In Vivo* Decoding Mechanisms of the Temporal Patterns of Blood Insulin by the Insulin-AKT Pathway in the Liver, Cell Systems (2018), https://doi.org/10.1016/j.cels.2018.05.013

Cell Systems
Article

In Vivo Decoding Mechanisms of the Temporal Patterns of Blood Insulin by the Insulin-AKT Pathway in the Liver

Hiroyuki Kubota,[1,2,5,*] Shinsuke Uda,[1] Fumiko Matsuzaki,[1] Yukiyo Yamauchi,[1] and Shinya Kuroda[3,4,*]
[1]Division of Integrated Omics, Research Center for Transomics Medicine, Medical Institute of Bioregulation, Kyushu University, 3-1-1 Maidashi, Higashi-ku, Fukuoka, Fukuoka 812-8582, Japan
[2]PRESTO, Japan Science and Technology Agency, Higashi-ku, Fukuoka, Fukuoka 812-8582, Japan
[3]Department of Biological Sciences, Graduate School of Science, University of Tokyo, Bunkyo-ku, Tokyo 113-0033, Japan
[4]CREST, Japan Science and Technology Corporation, Bunkyo-ku, Tokyo 113-0033, Japan
[5]Lead Contact
*Correspondence: kubota@bioreg.kyushu-u.ac.jp (H.K.), skuroda@bs.s.u-tokyo.ac.jp (S.K.)
https://doi.org/10.1016/j.cels.2018.05.013

SUMMARY

Cells respond to various extracellular stimuli through a limited number of signaling pathways. One strategy to process such stimuli is to code the information into the temporal patterns of molecules. Although we showed that insulin selectively regulated molecules depending on its temporal patterns using Fao cells, the *in vivo* mechanism remains unknown. Here, we show how the insulin-AKT pathway processes the information encoded into the temporal patterns of blood insulin. We performed hyperinsulinemic-euglycemic clamp experiments and found that, in the liver, all temporal patterns of insulin are encoded into the insulin receptor, and downstream molecules selectively decode them through AKT. S6K selectively decodes the additional secretion information. *G6Pase* interprets the basal secretion information through FoxO1, while GSK3β decodes all secretion pattern information. Mathematical modeling revealed the mechanism via differences in network structures and from sensitivity and time constants. Given that almost all hormones exhibit distinct temporal patterns, temporal coding may be a general principle of system homeostasis by hormones.

INTRODUCTION

Cells regulate various biological responses through a limited number of signaling pathways (Housden and Perrimon, 2014). To achieve this, cells can encode information into temporal patterns of molecules to regulate biological responses (Purvis and Lahav, 2013). Hormones have been shown to exhibit distinct temporal patterns (Brabant et al., 1992), and, in some cases, the patterns are important for their functions (Isaksson et al., 1985; Paolisso et al., 1988). For example, blood insulin exhibits several temporal patterns, such as additional secretion, which is a transient response observed in response to eating; basal secretion, which is a low constant secretion during fasting (Lindsay et al., 2003; Polonsky, 1988), and 10- to 15-min pulsatile secretion (O'Meara, 1993; O'Rahilly et al., 1988). These patterns are important for insulin actions (Bruce et al., 1988; Paolisso et al., 1988). In addition, relationships between insulin secretion abnormalities and type 2 diabetes mellitus (T2DM) have been reported (Pratley and Weyer, 2001; Prato, 2003). However, the mechanisms by which hormones regulate various biological responses via their temporal patterns remain unknown.

Insulin regulates various cellular responses. Among them, metabolic regulation, such as gluconeogenesis, glycogenesis, protein synthesis, and lipid synthesis, is a major target of insulin action and is regulated through the insulin-AKT (also known as protein kinase B [PKB]) signaling pathway and gene regulation *in vivo* (Whiteman et al., 2002; Yugi et al., 2014). Using rat hepatoma Fao cells, we have revealed that insulin selectively regulates the AKT pathway molecules, metabolism, and gene expression, via its temporal patterns (Kubota et al., 2012; Noguchi et al., 2013; Sano et al., 2016). However, as these results came from a cultured cell line, it remains unknown whether selective regulation by insulin exists in the liver or not. Moreover, the detailed mechanisms by which the insulin-AKT pathway processes the information of blood insulin patterns are not well understood.

In this study, we examined the *in vivo* responses of the insulin-AKT pathway molecules under hyperinsulinemic-euglycemic clamp conditions, and developed a mathematical model that reproduces the behavior of the molecules. We found that insulin selectively regulates the insulin-AKT pathway molecules depending on its temporal patterns in the liver, which is the organ most affected by insulin temporal patterns. We also found that the information encoded into the temporal patterns of insulin is transferred to AKT through the insulin receptor (IR) without much attenuation. The information was then simultaneously processed depending on the downstream molecules. Our study contributes to our understanding of the mechanisms not only of insulin but also of T2DM. Moreover, to our knowledge, this is the first simulation model that reproduced the behavior of the signaling pathway molecules by hormones *in vivo*. Given that almost all hormones exhibit distinct temporal patterns, our

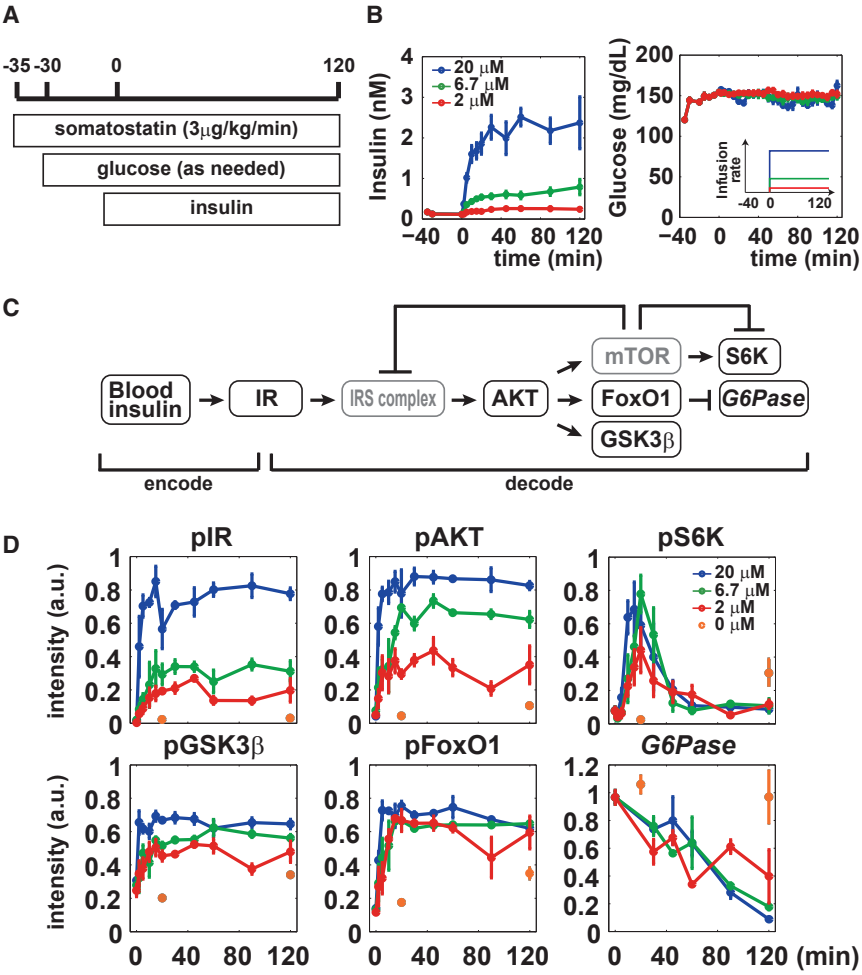

Figure 1. Different Temporal Patterns of pIR, pAKT, pS6K, pGSK3β, pFoxO1, and *G6Pase* in the Liver

(A) Schematic overview of experimental procedure. See details in Animal Procedures.

(B) Time courses of blood insulin and glucose level during step stimulation (inset). Blue, green, and red indicate time courses stimulated by 20, 6.7, and 2 μM insulin, respectively.

(C) Schematic overview of the insulin-AKT pathway.

(D) Insulin-induced time courses of pIR, pAKT, pS6K, pGSK3β, pFoxO1, and *G6Pase* in the liver. The means and SEMs of three independent experiments are shown.

study demonstrates the possibility of temporal coding as a general principle of system homeostasis by hormones.

RESULTS

The Insulin-AKT Pathway Molecules Captured Distinct Properties of Blood Insulin Patterns

We measured the insulin-AKT pathway molecules in the liver under hyperinsulinemic-euglycemic clamp conditions by administering insulin through the mesenteric vein and glucose and somatostatin through the jugular vein (Figures 1A and 1B and STAR Methods). We administered somatostatin through the jugular vein to suppress endogenous insulin secretion. We first administered insulin at a constant infusion rate, using the indicated doses, denoted as "step" stimulation (Figure 1B). The blood insulin concentration increased and reached a steady state around 20 min after insulin administration, which covered the physiological range of insulin (0.1–2.5 nM) (Jaspan et al., 1986; Song, 2000) (Figures 1B and S1A). The amount of infused glucose depended on the insulin concentration (Figure S1A); therefore, the insulin response *in vivo* was considered normal within this insulin concentration range.

In our previous study, we did not measure phosphorylated IR (pIR) and phosphorylated forkhead box protein O1 (pFoxO1). However, these molecules are also important in understanding the selective regulation mechanisms of the insulin-AKT pathway, because IR is a "sole receptor" of the cell for insulin, and FoxO1 regulates many gene expressions. Therefore, in this study, we measured pIR and pFoxO1 in addition to phosphorylated AKT (pAKT), phosphorylated S6K (pS6K), phosphorylated GSK3β (pGSK3β), and the amount of *G6Pase* (Figures 1C, 1D, and S1B). The step stimulation by insulin induced sustained increases in pIR, pAKT, pGSK3β, and pFoxO1, in an insulin-dose-dependent manner, while their sustained responses were different against different insulin doses. *G6Pase*, a downstream molecule of pFoxO1, showed a gradual decrease, regardless of the insulin dose. pS6K, another downstream molecule of pAKT, showed transient responses. As control, PBS stimulation without insulin was performed. Blood insulin did not increase (Figure S1C), while pAKT, pS6K, pGSK3β, and pFoxO1 showed slight increases at 120 min (Figure 1D), suggesting that these responses are not caused by insulin but rather likely by the side effect of anesthesia and/or euglycemic clamp conditions. The responses of pAKT, pS6K, pGSK3β, and pFoxO1 caused by insulin stimulation were much larger than those caused by control stimulation. Moreover, previous inhibitor and knockout mouse studies have shown that pS6K, pGSK3β, pFoxO1, and *G6Pase* were dominantly regulated by AKT (Humphrey et al., 2013; Kubota et al., 2012; Okamoto et al., 2007). Therefore, we assume that the molecules are dominantly regulated by insulin. These responses to insulin step stimulation *in vivo* are consistent with those in rat hepatoma Fao cells and primary hepatocytes (Kubota et al., 2012), except that no transient responses of pAKT and pGSK3β were observed *in vivo*. However, considering that the temporal patterns of pAKT are different between the liver and Fao cells, the regulation mechanisms between them are different. The measured molecules showed distinct temporal patterns in response to the step stimulation by insulin, indicating that the insulin-AKT pathway molecules captured distinct properties of the temporal patterns of insulin.

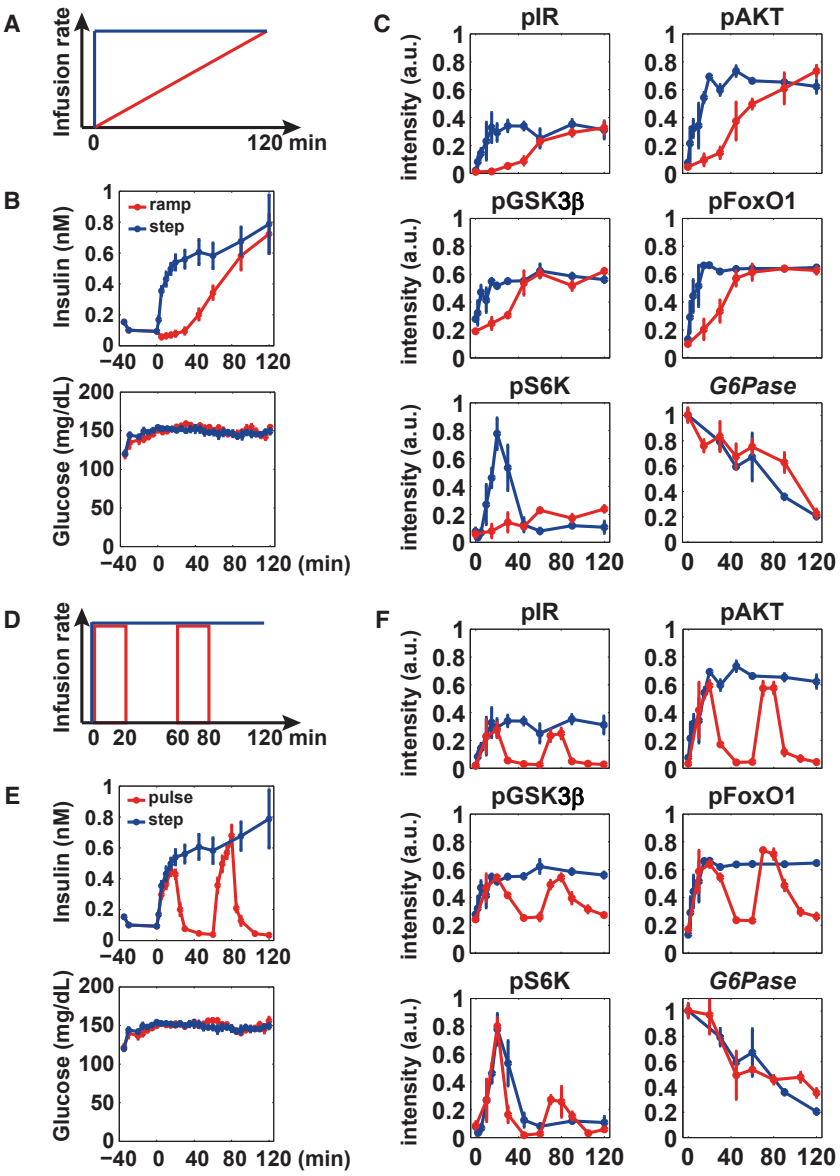

Figure 2. Final Amplitude and the Increasing Rate of Insulin Are Encoded into the Temporal Patterns of the Molecules

(A) Infused patterns of ramp (red) and step (blue) stimulation using 6.7 μM insulin.

(B) Time courses of blood insulin and glucose level stimulated by ramp (red) and step (blue) stimulation.

(C) Insulin-induced time courses of pIR, pAKT, pS6K, pGSK3β, pFoxO1, and *G6Pase* in the liver stimulated by ramp (red) and step (blue) stimulation. The means and SEMs of three independent experiments are shown.

(D) Infused patterns of pulse (red) and step (blue) stimulation using 6.7 μM insulin.

(E) Time courses of blood insulin and glucose level stimulated by pulse (red) and step (blue) stimulation.

(F) Insulin-induced time courses of pIR, pAKT, pS6K, pGSK3β, pFoxO1, and *G6Pase* in the liver stimulated by pulse (red) and step (blue) stimulation. The means and SEMs of three independent experiments are shown. Note that the results of the step stimulation are the same as those in Figure 1 (the results of 6.7 μM insulin stimulation).

Selective Encoding of Different Temporal Patterns by the Insulin-AKT Pathway Molecules

We examined the responses of the molecules using a gradually increasing stimulation, denoted as "ramp" stimulation (Figures 2A–2C, red). In response to ramp stimulation, pIR, pAKT, pGSK3β, and pFoxO1 increased, and *G6Pase* decreased, reaching the same final amplitudes as those in response to the step stimulation, indicating that their sustained responses capture the information concerning insulin concentration (Figures 2C and S2A). Previously, we observed that the transient response of pS6K depended on the increasing rate of insulin (Kubota et al., 2012). In this study, we also showed that the transient response of pS6K decreased in response to ramp stimulation (Figure 2C). This indicated that the transient response of pS6K also depends on the increasing rate of insulin *in vivo*. In addition, the final amplitude of pS6K observed with ramp stimulation was larger than that observed with step stimulation. The reason for this seems to be that the blood insulin concentration was increasing, even at 120 min, during ramp stimulation, whereas it did not increase at this time point during step stimulation (Figures 2B and 2C). Alternatively, since pS6K showed a similar weak increase at 120 min by ramp insulin stimulation and by control PBS stimulation (Figures 1D and 2C), suggesting that the weak increase of pS6K at 120 min may not be caused by the ramp insulin stimulation but rather by the side effects of the unknown experimental conditions. These results indicated that pS6K does not capture the final concentration of insulin, whereas it responds to the increasing rate. The initial rate of change of all molecules except *G6Pase* by ramp stimulation became slower than those observed by step stimulation, while the initial decreasing rates of *G6Pase* were similar during both step and ramp stimulation. Different from Fao cells, these results indicated that the initial increasing rate of molecules captured the increasing rate of insulin, rather than the final concentrations. On the other hand, the final amplitude of all molecules except pS6K by ramp stimulation reached the same final amplitude as those by step stimulation. These results also indicate that the final amplitude of molecules captured the final concentration of insulin, rather than its increasing rate.

Next, we further examined the responses of the molecules using two pulses of stimulation, denoted as "pulse" stimulation (Figures 2D–2F, red). In response to pulse stimulation, pIR, pAKT, pGSK3β, and pFoxO1 showed similar responses to the temporal patterns of insulin (Figures 2E and 2F), indicating that these molecules can quickly follow the temporal changes in insulin concentrations. By contrast, *G6Pase* showed a continuous decrease and did not show a pulse-like pattern (Figure 2F).

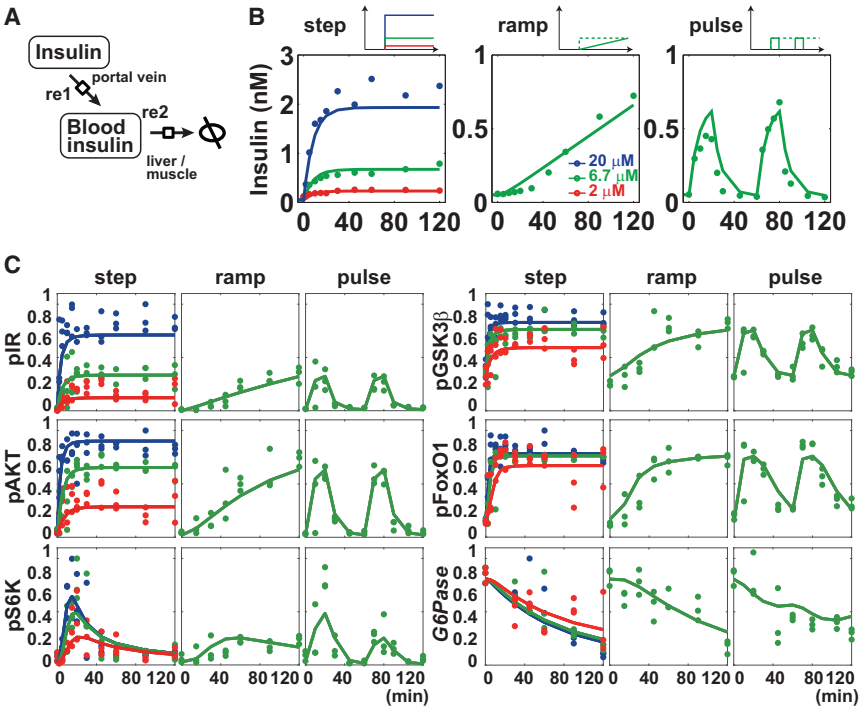

Figure 3. Development of *In Vivo* Insulin-Dependent Insulin-AKT Pathway Model

(A) Schematic overview of the blood insulin model. See details in Simulation and Parameter Estimation.

(B) Time courses of blood insulin concentration in step, ramp, and pulse stimulations. Lines and dots indicate simulation and experimental results, respectively. Blue, green, and red indicate time courses stimulated by 20, 6.7, and 2 μM insulin, respectively.

(C) Insulin-induced time courses of pIR, pAKT, pS6K, pGSK3β, pFoxO1, and *G6Pase* in step, ramp, and pulse stimulation. Lines and dots indicate simulation and experimental results, respectively.

The fact that only upstream pFoxO1, but not downstream *G6Pase*, could respond to pulse stimulation strongly suggested that the response of *G6Pase* to pFoxO1 is so slow that *G6Pase* cannot follow the temporal changes in insulin concentrations. pS6K showed similar responses to pIR, pAKT, pGSK3β, and pFoxO1 with regard to the temporal patterns of insulin, except for a weak second transient peak (Figure 2F). However, given that pS6K responds to the increasing rate of insulin, rather than its final concentration (Figure 2C), the response of pS6K to pulse stimulation also depends on the increasing rate of insulin. By contrast, the responses of pIR, pAKT, pGSK3β, and pFoxO1 to pulse stimulation depend on the insulin concentration, which also means that these molecules quickly follow the temporal patterns of upstream molecules. Taken together, the results show that pIR, pAKT, pGSK3β, and pFoxO1 respond quickly and *G6Pase* responds slowly to the insulin concentration, while pS6K responds to the increase rate of insulin in the liver.

Development of the Insulin-AKT Pathway Model

We developed a blood insulin model (Figures 3A, 3B, S3A, and S3B, Data S1, and Simulation and Parameter Estimation). The model reproduced the experimental data of the sustained responses to step stimulation, the continuous increase induced by ramp stimulation, and two pulses induced by pulse stimulation (Figure 3B). Next, we developed the insulin-AKT pathway model (Figures 1C, 3C, S3C, S3D, S4, and S5, Data S1, and Simulation and Parameter Estimation), where insulin in the model of blood insulin was used as an input. The insulin-AKT pathway model was developed based on our previous AKT pathway model in Fao cells (Kubota et al., 2012) except for three major changes (Figure 1C, and Simulation and Parameter Estimation). The first one is an addition of IR. This addition enables us to understand the information processing mechanism of blood insulin pattern through IR, which we could not reveal in the previous study. The second one is a regulation of insulin receptor substrate (IRS). Although it is reported that the amount of IRS is decreased in response to insulin, under our experimental condition within 2 hr, the amount of IRS did not significantly decrease. Therefore, we did not include this assumption in the current model. The third one is a regulation of GSK3β. We found that there was another regulation mechanism except AKT from the model analysis. The insulin-AKT pathway model reproduced the experimental results of all molecules, including pIR, pAKT, pGSK3β, pFoxO1, pS6K, and *G6Pase*, in response to step, ramp, and pulse stimulation (Figure 3C), indicating that our model captures the essential features of the insulin-AKT pathway molecules (Figure S3C). In particular, the model reproduces the second weak transient response of pS6K during pulse stimulation. This indicated the validity of the network structure of pS6K; i.e., acting via the incoherent feed-forward loop (IFFL). Note that, although we assumed IFFL to reproduce the characteristics of pS6K in this model, similar characteristics can also be seen in a negative feedback loop.

Selective Decoding Mechanisms by the Insulin-AKT Pathway Molecules

The temporal patterns of insulin were encoded into an activity of "a gate" of the cell for insulin, the IR. The encoded information concerning pIR is further decoded by downstream molecules, such as pS6K, pGSK3, pFoxO1, and *G6Pase*, through AKT. We have found that information concerning insulin concentration and increasing rate was encoded into temporal patterns of these molecules (Kubota et al., 2012). To investigate how much information regarding insulin concentration is decoded into the sustained responses of these molecules, we quantified the sustained responses of all molecules against insulin concentration, using the step stimulation by constructing dose-response curves (Figure 4A). The dose-response curves of pIR, pAKT, pGSK3β, pFoxO1, and *G6Pase* at steady state showed monotonic increases, whereas that of pS6K revealed an adaptation response. These results indicated that pIR, pAKT, pGSK3β, pFoxO1, and

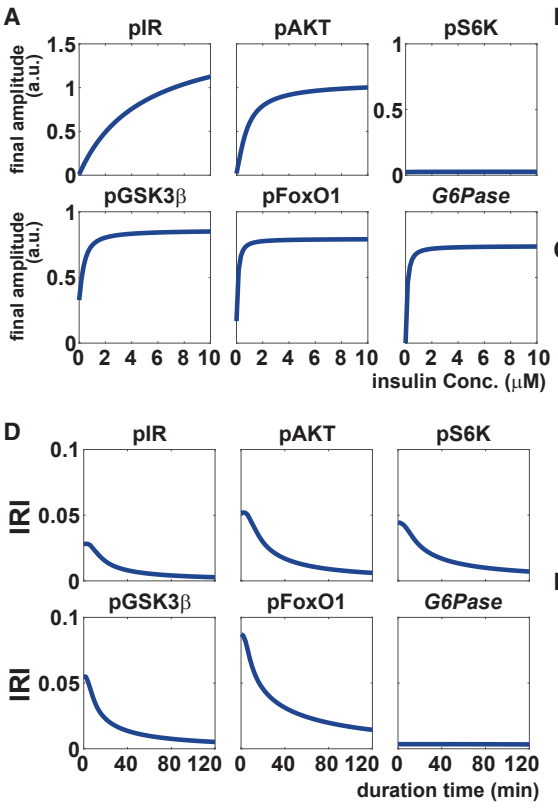

EC50s (nM)	pIR	pAKT
	4.874	0.835
pGSK3β	pFoxO1	*G6Pase*
0.360	0.107	0.107

pIR	pAKT	pS6K
0.0280	0.0517	0.0445
pGSK3β	pFoxO1	*G6Pase*
0.0550	0.0872	0.0035

Figure 4. Encoding of the Insulin Temporal Patterns into the Insulin-AKT Pathway

(A) The final amplitudes of the indicated molecules were plotted against insulin in the simulation.

(B) The EC_{50}s of the indicated molecules.

(C) The definition of increasing rate indexes (IRIs).

(D) IRIs for the molecules against the increasing rate of insulin.

(E) Dynamic range of IRI for the indicated molecules.

G6Pase, but not pS6K, decode the information regarding the insulin concentration into their sustained responses. The half-maximal concentrations (EC_{50}s) against insulin of pIR, pAKT, pGSK3β, pFoxO1, and *G6Pase* were 4.874, 0.835, 0.360, 0.107, and 0.107, respectively (Figure 4B). Its large EC_{50} means that pIR can encode a wide range of insulin concentration information. By contrast, because of their small EC_{50}s, pFoxO1 and *G6Pase* showed the highest sensitivity and maximal response even at low concentrations of insulin. These results indicated that the information concerning insulin concentration encoded into pIR is well transferred to pAKT and pGSK3β, and is not well transferred to pFoxO1 and *G6Pase*, whereas it is not transferred to pS6K.

As described above, the initial increasing rate of these molecules depended on the increasing rate of insulin (Figure 2C). To investigate how much information concerning insulin's increasing rate is decoded into the increasing rate of molecules, we quantified all molecules' rates against that of insulin using ramp stimulation (Figure 4C). We defined the increasing rate index (IRI), which is the time taken to change a molecule from 25% to 75% of the maximal response, as an index of the response to increasing rate of insulin (Figure 4D). The x axis of Figure 4D indicates the duration of ramp stimulation, which is inversely proportional to the increasing rate of stimulation; a smaller ramp duration indicates faster increasing rate. As the increasing rate of insulin decreased, the IRIs of the molecules decreased, except for *G6Pase* (Figures 4D and S6B), indicating that increasing rate of insulin is decoded into an increasing rate of the molecule. Since all IRIs converge to 0, the dynamic range of IRI was calculated at time = 0, which indicates how much information regarding the increasing rate of insulin is transferred. A molecule with a larger IRI shows a larger dynamic range of increasing rate of insulin. The IRIs of pIR, pAKT, pS6K, pGSK3β, pFoxO1, and *G6Pase* were 0.0280, 0.0517, 0.0445, 0.0550, 0.0872, and 0.0035, respectively (Figure 4E). The molecules with the largest and smallest IRIs were 0.0872 (pFoxO1) and 0.0035 (*G6Pase*), respectively. Therefore, at this dose, information concerning increasing rate of insulin was well transferred to pFoxO1, whereas it was not well transferred to *G6Pase*. Moreover, even if the increasing rate of insulin decreased, the IRI of *G6Pase* hardly changed (Figure 4D). This indicated that the information concerning increasing rate of insulin is not well transferred to *G6Pase*.

Following the Insulin Patterns

We quantified the similarities of temporal patterns between insulin and the molecules using correlation, which is a simple measure of how the molecules follow the temporal changes of insulin. Assuming that the information is encoded into the temporal patterns of blood insulin, knowing how much the patterns are transferred to downstream molecules is important from the viewpoint of information transfer. In short, if a temporal pattern of a downstream molecule is the same as that of an upstream molecule, it is considered that all information from the upstream molecule is transferred to the downstream one. Therefore, we used correlation, which is a simple measure of similarity, for temporal patterns, assuming that the insulin signaling pathway does not carry out complicated information processing. To investigate how much the insulin-AKT pathway molecules resemble the blood insulin patterns, we defined the similarity index (SI) (Figure 5A), which is the absolute value of the correlation coefficient between insulin and a molecule. We calculated the SIs using simulation and experimental data from step, ramp, and pulse stimulations (Figure 5B). The SIs of pIR, pAKT, pGSK3β, and pFoxO1 were large (>0.5) in both the simulations and experiments; therefore, the temporal patterns of these molecules were similar to those of insulin. On the other hand, as the SIs of pS6K and *G6Pase* were small (<0.4), the temporal patterns of these molecules were not similar to those of insulin. The network structure of pS6K is an IFFL. This explains why the temporal pattern of pS6K was not similar to that of insulin, because

A

SI = |correlation|

B

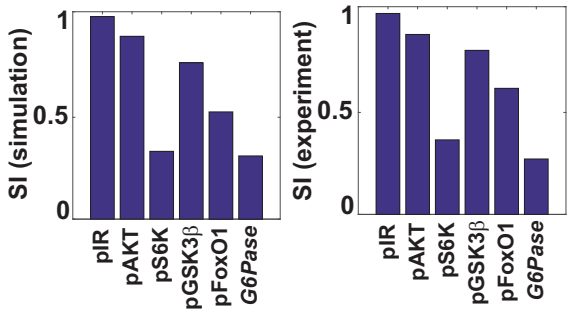

C

time constant (min)	pIR	pAKT
	3.13	3.81
pGSK3β	pFoxO1	*G6Pase*
2.20	3.91	74.0

Figure 5. Following the Molecules against the Temporal Patterns of Insulin

(A) The definition of Similarity Indexes (SIs).

(B) The SIs of the indicated molecules in simulation (left panel) and experiments (right panel).

(C) The apparent time constant (tau) of the indicated molecules.

pS6K responds to the increasing rate of insulin, rather than its concentration. Contrastingly, the network structure of *G6Pase* is a feed-forward structure (FF), which is the same as that of pIR, pGSK3β, and pFoxO1. We supposed that the difference between *G6Pase* and others lies in the speed of their responses. Therefore, we calculated the apparent time constants, which are defined as the time to reach 63.2% of the steady state by step stimulation of the input by approximating a linear first-order system. The apparent time constants of pIR, pAKT, pGSKβ, pFoxO1, and *G6Pase* against insulin were 3.13, 3.81, 2.20, 3.91, and 74.0 min, respectively (Figure 5C), indicating that *G6Pase* is much slower than the others. This is the reason why only *G6Pase*, but not the other molecules, can follow changes in insulin. This difference in time constants is likely to occur because of differences in the regulation mechanism; *G6Pase* is regulated through gene expression, which is a relatively slow process, whereas the others are regulated by phosphorylation, which is a faster process. We confirmed whether the SI of *G6Pase* increased by decreasing the increasing rate of insulin using ramp stimulation (Figure S7A). As the increasing rate of insulin decreased, the SI of *G6Pase* increased and reached almost 1. Hence, if the increasing rate of insulin is sufficiently small compared with the apparent time constant of *G6Pase*, its temporal patterns would be similar to that of insulin. Also, the reason why *G6Pase* exhibited a similar pattern to step stimulation when stimulated by pulse stimulation was as follows: *G6Pase* could not return to the basal level after the first stimulation because of the large apparent time constant and subsequently responded to the second stimulation. The apparent time constant of *G6Pase* in response to insulin is far larger than that of pFoxO1 (Figure 5C). Therefore, we calculated the apparent time constant of *G6Pase* against pFoxO1 and found that it was 70.22 min (Figure S7B), which is almost the same as that against insulin (Figure 5C). This indicated that the large time constant is dependent on the step between FoxO1 and *G6Pase*. Considering the results above, the characteristic of *G6Pase* depends on two steps: a small EC_{50} from insulin to pFoxO1 and a large apparent time constant from pFoxO1 to *G6Pase*.

Responses to the *In Vivo* Temporal Patterns

It is reported that blood insulin exhibits 10- to 15-min pulsatile secretion (O'Meara, 1993; O'Rahilly et al., 1988), additional secretion, and basal secretion (Lindsay et al., 2003; Polonsky, 1988), and these patterns are important for insulin actions. The additional secretion is a pulse-like secretion whose duration is about 2 hr. The basal secretion is a low constant secretion during fasting that occurs on the scale of 1 day. We examined how the insulin-AKT pathway molecules responded to the *in vivo*-like patterns using a sinusoidal wave (Stim_sin) (Figures 6A, 6B, and S8A). We used a sinusoidal wave with a period of 15 min, 2 hr, and 24 hr, which resembles the 10- to 15-min pulsatile secretion, additional secretion, and basal secretion, respectively (Figure S8A). We used two stimulation patterns as controls (Figures 6A and S8A). One was a step stimulation whose maximal amplitude is the same as that of the Stim_sin (Stim_max). The other was a step stimulation in which the amount of administered insulin per time is the same as that of the Stim_sin (Stim_adm). To quantify the maximal response of Stim_sin (Peak_sin), we defined the peak ratio index (PRI) (Figure 6A); PRI indicates the difference between the peak value of Stim_max (Peak_max) and Stim_adm (Peak_adm), which is normalized to 1. The reasons why we used the PRI rather than an index based on the area under the curve (AUC) were as follows: (1) the peak of a molecule is thought to reflect the activity of the molecule, (2) AUC seemed not to capture the characteristics well among the different insulin stimulation patterns (Figure S8D). If the PRI of Peak_sin is 1 or 0, it shows the same value as Peak_max or Peak_adm, respectively. In addition, if the PRI of Peak_sin is over 1 or below 0, the Peak_sin exceeds the Peak_max value or has a value that does not reach the Peak_adm, respectively. The relationship of the amount of administrated insulin per time among the stimulation patterns was as follows:

$$\text{Stim\_adm} = \text{Stim\_sin} = \text{Stim\_max}/2$$

The PRIs of pIR, pAKT, pGSK3β, and pFoxO1 in response to stimulation period of 15 min were 0.59, 0.49, 0.53, and 0.37, respectively (Figure 6B). As the period of sinusoidal wave was increased, the PRIs of pIR, pAKT, pGSK3β, and pFoxO1 increased and reached almost 1 (Figure 6B). The PRIs of *G6Pase* in response to stimulation period of 15 min and 2 hr were about 0, and reached almost 1 in response to stimulation period of 24 hr. The PRI of pS6K in response to stimulation period of 15 min was 0.13. Unlike the other molecules, the PRI of pS6K showed a maximum at stimulation period of 2 hr (0.48), but decreased below 0 at a stimulation period of 24 hr. These results indicated that pIR, pAKT, pGSK3β, and pFoxO1 adequately respond to a stimulation period of 15 min, and respond sufficiently to those of 2 and 24 hr. Note that, even if we changed the insulin concentration, the overall characteristics of PRIs were similar. Therefore, these molecules may adequately respond to the 10- to 15-min pulsatile, and to the additional and

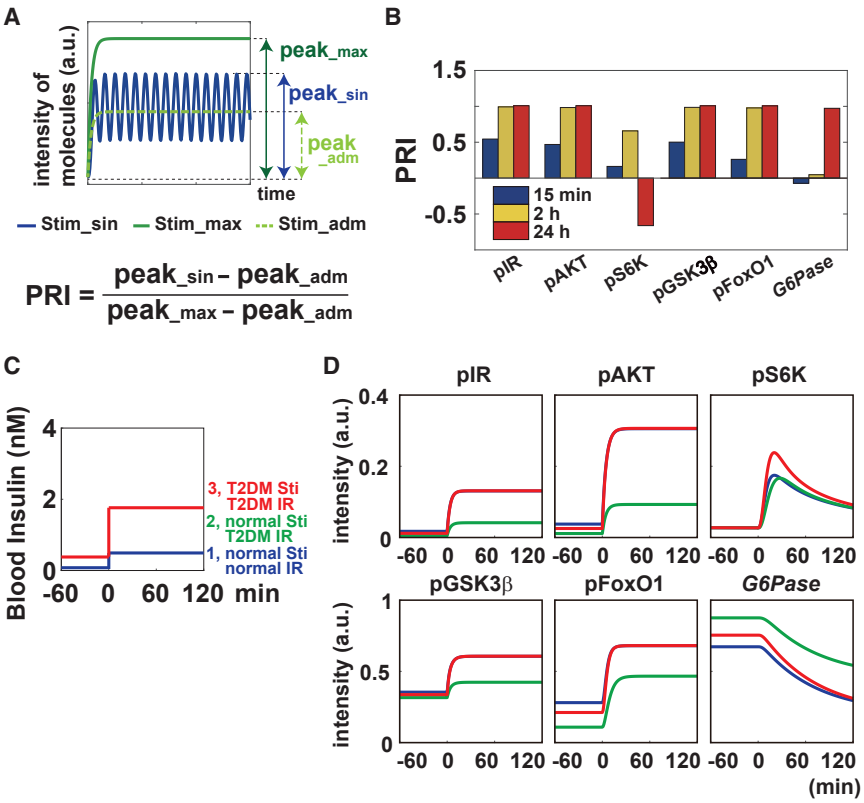

Figure 6. Responses to *In Vivo*-Like Insulin Temporal Patterns

(A) The definition of peak ratio indexes (PRIs). Peak_max, Peak_adm, and Peak_sin indicate the peak of Stim_max, Stim_adm, and Stim_sin, respectively. Stim_sin indicates the time course of the molecules stimulated by the indicated insulin sinusoidal waves with different frequencies. Stim_max indicates a control step stimulation, whose maximal amplitude is the same as that of the Stim_sin. Stim_adm indicates another step control stimulation, whose amount of administered insulin per time is the same as that of the Stim_sin.

(B) The PRIs for the molecules with a period of 15 min (blue), 2 hr (yellow), and 24 hr (red). See also Figure S8A.

(C) Three-step stimulation patterns of insulin: blue, green, and red lines indicate the normal IR phosphorylation activity and normal insulin stimulation, one-third of the normal IR phosphorylation activity and normal insulin stimulation, and one-third of the normal IR phosphorylation activity, and 3.5 times insulin stimulation patterns, respectively. Note that the green line is overlapped with the blue line.

(D) Time courses of pIR, pAKT, pS6K, pGSK3β, pFoxO1, and *G6Pase* induced by the three stimulation patterns above. Note that the sustained responses of blue lines in pIR, pAKT, pGSK3β, and pFoxO1 are overlapped with red lines.

basal, secretions *in vivo*. *G6Pase* could not respond sufficiently to stimulation period of 15 min and 2 hr, indicating that it could only respond in the same way as that of the Stim_adm, a low step control. However, *G6Pase* responded efficiently to stimulation period of 24 hr. These simulation results indicate that *G6Pase* cannot respond efficiently to the 10- to 15-min pulsatile secretion and the additional secretion, whereas it can respond efficiently to the basal secretion *in vivo*. However, this is the simulation result from the sinusoidal stimulation at the steady-state condition. To further confirm the characteristics, we need to perform sinusoidal stimulation under the steady-state-like condition *in vivo*. pS6K could not respond sufficiently to stimulation period of 15 min. Unlike the other molecules, pS6K responded adequately to stimulation period of 2 hr but could not respond to that of 24 hr. These results indicated that pS6K responds efficiently to the additional secretion whose duration is about 2 hr, whereas it cannot respond to the basal secretion *in vivo*. Thus, blood insulin selectively regulates the insulin-AKT pathway molecules depending on its *in vivo* temporal patterns.

Impairment of IR activity and reducing the amount of IR were reported to cause insulin resistance (Burant et al., 1986; Kubota et al., 2017). In addition, these IR abnormalities were reportedly related to T2DM (Bruce et al., 1988; O'Rahilly et al., 1988; Pratley and Weyer, 2001; Prato, 2003). Therefore, we next examined the responses of molecules to simulation of the early stages of T2DM (Figures 6C, 6D, S8B, and S8C). It is reported that the ratio between the peak of the additional and basal secretion remains the same between normal and T2DM patients (Lindsay et al., 2003; Polonsky, 1988). Therefore, we made their ratio the same in the following stimulation patterns. We used three types of conditions, as follows: normal IR phosphorylation activity (k3 in Figure S4) with normal insulin stimulation (condition 1; blue lines), one-third of the normal IR phosphorylation activity with normal insulin stimulation (condition 2; green lines), and one-third of the normal IR phosphorylation activity with 3.5 times higher insulin concentration in both basal and stimulation conditions (condition 3; red lines) (Figure 6C). Compared with the normal condition (condition 1), in response to condition 2, responses of all the molecules decreased (Figure 6D), indicating insulin resistance. Thus, reducing the IR phosphorylation activity is enough to decrease the responses of all the insulin-AKT pathway molecules. If the amount of insulin stimulation increased under reduced IR phosphorylation activity (condition 3), the responses of all the molecules recovered (Figure 6D). However, the basal level of pFoxO1 and *G6Pase* did not return to normal, even if we increased the basal insulin concentration, whereas those of the other molecules were almost the same. The same results were obtained even if we decreased IR expression level (Figures S8B and S8C). These results indicated that impairment of the insulin-AKT pathway molecules caused by IR abnormalities could be compensated for by changes in blood insulin patterns.

DISCUSSION

Information Processing by the Insulin-AKT Pathway Molecules

We showed how the information encoded in the temporal patterns of insulin, concentration and the increasing rate, was

Please cite this article in press as: Kubota et al., *In Vivo* Decoding Mechanisms of the Temporal Patterns of Blood Insulin by the Insulin-AKT Pathway in the Liver, Cell Systems (2018), https://doi.org/10.1016/j.cels.2018.05.013

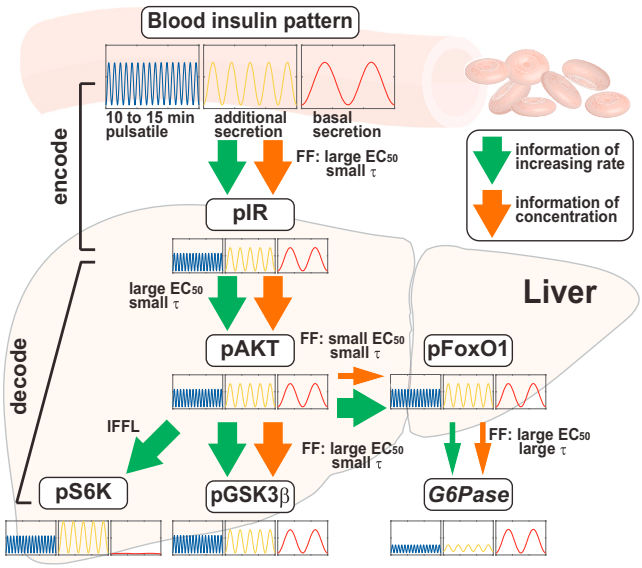

Figure 7. Encoding and Decoding of the Blood Insulin Patterns in the Insulin-AKT Pathway

The information concerning the increasing rate and concentration encoded into the insulin temporal patterns is transferred until pAKT without much attenuation because of the large EC_{50} and small apparent time constant (τ). Then, pS6K selectively decodes the information concerning the increasing rate of insulin by the characteristic of an IFFL. pGSK3β decodes all information by the characteristics of an FF, with a large EC_{50} and small apparent time constant. pFoxO1 decodes the information concerning increasing rate of insulin by the characteristics of an FF, with a small EC_{50} and small apparent time constant. *G6Pase* decodes a little information regarding the insulin concentration (switch-like response) by the characteristics of an FF, with a large EC_{50}, through pFoxO1.

processed and transferred by the insulin-AKT pathway, using both biological experiments and a mathematical model (Figure 7). In this paper, the similarity in the temporal patterns between upstream and downstream molecules is one of the indexes of how much information is transferred from the upstream molecule to the downstream molecule. Note that the reverse is not necessarily true; information can be transferred without much loss if there is complicated information processing (see below). If the temporal pattern of the downstream molecule is different from that of the upstream molecule, this indicates that there is some information processing between them. To quantify this, we used the SI, defined as the absolute value of the correlation coefficient between insulin and a molecule. We used correlation because it is a simple measure of similarity for temporal patterns, assuming that the insulin signaling pathway does not carry out complicated information processing. However, if a signaling pathway carries out complicated information processing, we should use another index, such as mutual information (Filippi et al., 2016; Uda et al., 2013). Considering that IR is an sole receptor of the cell for insulin to transfer the information, blood insulin should encode as much information into pIR as possible. The EC_{50} and apparent time constant of pIR are large and small, respectively (Figures 4B, 5C, and 7). In addition, the SIs of pIR in both the simulation and the experiments were the largest (Figure 5B). These results indicated that blood insulin (outside the cell) encodes much information into pIR (inside the cell). AKT is a fork in the insulin-AKT pathway; therefore, much information should be transferred to AKT. The EC_{50} and apparent time constant of pAKT were relatively large and small, respectively (Figures 4B, 5C, and 7). Additionally, the SIs of pAKT in both the simulation and the experiments were the second largest (Figure 5B). Therefore, the information concerning the insulin concentration and increasing rate was encoded into the temporal patterns of insulin, which was transferred to AKT without much attenuation. The exquisite mechanisms of information transfer by the signaling pathway were first revealed by this study. The information was then processed differently, depending on the downstream molecules. The EC_{50} and apparent time constant of GSK3β against AKT are larger and smaller than those of pFoxO1, respectively (Figures S6A, S7B, and 7). Consequently, GSK3β can respond more quickly and with a wider dynamic range than pFoxO1, indicating that GSK3β receives more information from AKT compared with pFoxO1. The SI of GSK3β was the third largest (Figure 5B). By contrast, as the EC_{50} and apparent time constant of FoxO1 against AKT were small (Figures S6A, S7B, and 7), pFoxO1 similarly responded to both a low and high concentration of pAKT. This is one explanation for why the SI of pFoxO1 was smaller than that of GSK3β. Subsequently, as the apparent time constant of *G6Pase* against FoxO1 is large (Figures S7B and 7), the increasing rate of *G6Pase* did not change, even if the stimulation speed was fast or slow (Figure 2C). However, because of the small EC_{50} of pFoxO1 against insulin, *G6Pase* also responds to low insulin concentrations. This is the reason why the SI of *G6Pase* was small (Figure 5B). These differences are thought to be important for further information processing (Behar et al., 2008). The temporal pattern of pS6K was totally different from others because of the network structure (IFFL). The characteristics of the IFFL mean that pS6K decodes information concerning increasing rate but not its concentration (Figures S3C, S3D, S4, S5, and 7). Therefore, pS6K cannot follow the changes of the insulin patterns. This is the reason why the SI of pS6K was small (Figure 5B). There are many kinds of molecules in the insulin-AKT pathway, and their temporal patterns are reportedly different (Humphrey et al., 2013, 2015). Therefore, other molecules might also be selectively regulated in the same way. In case of a direct kinase-substrate relationship, potential mechanisms of selective regulation are thought to be derived from differences of affinities against the substrates, different phosphatase, and/or molecular localization. In particular, if an activity of phosphatase become stronger, a time constant will become smaller, and vice versa. The value of EC_{50} is determined by a balance between kinase and phosphatase activity. It is known that molecules related to lipid metabolism are also regulated by the insulin-AKT pathway, such as phosphorylation of ACLY (Humphrey et al., 2013), and gene regulation of FASN and ACC (Wang et al., 2015). In our study, we did not observe the responses of these molecules. However, temporal patterns of insulin are thought to be also important in the regulation of these molecules. These parallel information processing mechanisms are thought to be a common feature of the signaling pathway.

pS6K responds selectively to the additional secretion but not to the basal secretion pattern (Figure 7). Considering that S6K regulates protein synthesis, S6K accelerates protein synthesis in response to the additional secretion after the meals. In

particular, because a certain interval of the stimulation is necessary for effective activation of S6K, we may need an interval between meals for effective protein synthesis in daily life. It is reported that S6K is regulated not only by insulin but also by amino acid through mTORC1. Although we did not consider the effect of amino acid in this study, amino acid may affect the basal activity and/or amplitude of pS6K. *G6Pase* preferentially responds to the basal secretion pattern (Figure 7). Considering that *G6Pase* regulates gluconeogenesis, it may be regulated by slow changes of insulin over a day. Gluconeogenesis is regulated in hours by meals. It is reported that adipocyte lipolysis is more important than transcriptional regulation by FoxO1 in the regulation of gluconeogenesis *in vivo* (Perry et al., 2015; Titchenell et al., 2016). We showed that *G6Pase* expression is regulated in days rather than in hours (Figures 6B and S8A). This is consistent with the results of the previous studies above. Therefore, changes in *G6Pase* expression may be important for regulation in days rather than that in hours. Moreover, as the EC_{50} of *G6Pase* against insulin is small, *G6Pase* shows a switch-like response against insulin. Considering that *G6Pase* is suppressed in response to insulin, maintaining a small amplitude of insulin for a long time, such as in basal secretion, may be necessary for gluconeogenesis activation. The response of *G6Pase* to the basal insulin under IR abnormal conditions was still higher than that under normal conditions because of its high sensitivity against insulin, whereas those of the other molecules, except pFoxO1, were almost the same (Figure 6D, red and blue). This indicated that *G6Pase* and pFoxO1 might be more sensitive to changes in concentration around the basal secretion level compared with the other molecules. This may be one of the reasons why the fasting blood glucose level in patients at the early stage of T2DM is high. pGSK3β responds to all secretion patterns (Figure 7). Considering that pGSK3β regulates glycogenesis, pGSK3β might need to rapidly regulate glycogenesis in response to insulin, because glycogenesis is directly related to blood glucose regulation.

The insulin-AKT pathway molecules in the liver can more efficiently respond to the blood insulin patterns than those in the Fao (Kubota et al., 2012). One of the reasons is the differences in the parameters. For example, since pS6K in the liver returned to the basal level earlier (about 40 min) than that in Fao cells (6–8 hr), pS6K in the liver can more efficiently respond to the pulsatile stimulation, such as the additional secretion. The time constant of *G6Pase* against upstream molecules in the liver is larger (about 70 min) than that in the Fao cells (about 20 min). Therefore, *G6Pase* in the liver responds to the basal secretion rather than the additional secretion. Our model, which can reproduce *in vivo* behavior, will be necessary for drug discovery and prediction of T2DM, and may provide a proper understanding of insulin action in the liver.

pAKT, pS6K, pGSK3β, and pFoxO1, stimulated by 20-min control stimulation (0 nM insulin), did not change, whereas with 120 min they showed slight increases (Figure 1D). However, blood insulin did not increase with control stimulation (Figure S1C). Therefore, these changes are thought to be caused by non-insulin effects, such as anesthesia and/or euglycemic clamp conditions. Since a transient peak of pS6K was not observed by control stimulation, the transient peaks stimulated by insulin totally depended on the increasing rate of insulin. Also, since pAKT, pGSK3β, and pFoxO1 reached the steady state at around 20 min and did not change until 120 min, the indexes, such as EC_{50}, IRI, time constant, and PRI, reflect the characteristics of the molecules caused by insulin stimulation. Moreover, since the time course changes in pAKT, pS6K, pGSK3β, and pFoxO1 caused by insulin stimulation were much larger than those by control stimulation, these molecules are dominantly regulated by insulin. These results indicate that slight increases of pAKT, pS6K, pGSK3β, and pFoxO1 at 120 min from control stimulation do not affect our conclusions. However, we need to investigate further using a mathematical model.

In Vivo Temporal Coding

It is reported that cells regulate signaling pathways using temporal patterns of molecules. Although temporal pattern regulation at the intracellular (Dolmetsch et al., 1997; Hoffmann et al., 2002; Sasagawa et al., 2005; Vaudry et al., 2002) and intercellular levels (Urakubo et al., 2009) has been reported, there is no report on temporal regulation among organs. However, almost all hormones, including insulin, exhibit distinct temporal patterns (Brabant et al., 1992), and in some cases the patterns are important for their functions (Isaksson et al., 1985; Paolisso et al., 1988). In this study, we found that information concerning the concentration and increasing rate of insulin was encoded into the sustained and increasing rates of molecules, using both biological experiments and a mathematical model, respectively. It is reported that blood insulin exhibits several temporal patterns, such as the 10- to 15-min pulsatile secretion, additional secretion, and basal secretion (O'Rahilly et al., 1988; Polonsky, 1988). We found that pIR, pAKT, pGSK3β, and pFoxO1 could respond to all insulin patterns, pS6K could selectively respond to the additional secretion but not to the basal secretion, and *G6Pase* responds preferentially to the basal secretion (Figure 7). These results demonstrated the existence of temporal coding of insulin action *in vivo*. This is the first study, to our knowledge, to show this temporal coding and to reveal its mechanisms *in vivo*. Almost all hormones exhibit distinct temporal patterns; therefore, it is natural to think that other hormones also selectively regulate downstream molecules depending on their temporal patterns. Therefore, temporal coding is thought to be one of the common, basic mechanisms for selective regulation of biological responses *in vivo*.

We have found that insulin selectively regulates not only a signaling pathway but also metabolites and gene expression via its temporal patterns using rat hepatoma Fao cells (Kubota et al., 2012; Noguchi et al., 2013; Sano et al., 2016). Therefore, metabolites and gene expression might also be selectively regulated *in vivo*. It is reported that 13 min of pulsatile stimulation is more effective in decreasing the blood glucose level than continuous stimulation (Bratusch-Marrain et al., 1986; Grubert et al., 2005; Koopmans et al., 1996). There is a contradiction in patients with early-stage T2DM: the ability to suppress blood glucose levels decreases, whereas the liver stores a lot of fat in the patient, both of which are activated by insulin (Brown and Goldstein, 2008). Moreover, relationships between T2DM and insulin secretion abnormalities have been reported: the 10- to 15-min pulsatile secretion was diminished in patients with

Please cite this article in press as: Kubota et al., *In Vivo* Decoding Mechanisms of the Temporal Patterns of Blood Insulin by the Insulin-AKT Pathway in the Liver, Cell Systems (2018), https://doi.org/10.1016/j.cels.2018.05.013

T2DM (O'Rahilly et al., 1988), and the basal secretion increased (hyperinsulinemia) in patients with early-stage T2DM (Polonsky, 1988). The contradiction can be reasonably explained from the viewpoint of temporal coding: blood glucose and lipid synthesis are selectively regulated by the 10- to 15-min pulsatile secretion and basal secretion, respectively. In addition, we simulated the T2DM condition using our model by decreasing the activity and reducing the expression level of IR. In this simulation, we found that the responses of the insulin-AKT pathway molecules could be recovered to their normal levels by increasing the blood insulin concentration (Figures 6C, 6D, S8B, and S8C). This indicated that the responses of the insulin-AKT pathway molecules could be compensated for by changing insulin temporal patterns. It is reported that there are many causes of T2DM (Kubota et al., 2017). Abnormal blood insulin patterns in T2DM might contribute to the pathogenesis and/or progression of T2DM. Therefore, revealing the temporal coding mechanisms of insulin action is important to the understanding not only of insulin action but also the mechanism of T2DM.

STAR★METHODS

Detailed methods are provided in the online version of this paper and include the following:

- KEY RESOURCES TABLE
- CONTACTS FOR REAGENT AND RESOURCE SHARING
- EXPERIMENTAL MODEL AND SUBJECT DETAILS
  - Animal Procedures
- METHOD DETAILS
  - Western Blotting
  - RNA Isolation and Quantitative Real-Time Reverse Transcription PCR (qRT-PCR) Analysis
  - Simulation and Parameter Estimation
  - Definition of IRI, SI and PRI
- DATA AND SOFTWARE AVAILABILITY

SUPPLEMENTAL INFORMATION

Supplemental Information includes eight figures and one data file and can be found with this article online at https://doi.org/10.1016/j.cels.2018.05.013.

ACKNOWLEDGMENTS

This work was supported by PRESTO (Elucidation and Regulation in the Dynamic Maintenance and Transfiguration of Homeostasis in Living Body) from the Japan Science and Technology (JST) and Japan Society for the Promotion of Science (JSPS, KAKENHI grant number 16H06577). S.K. was funded by CREST (Creation of Fundamental Technologies for Understanding and Control of Biosystem Dynamics, JPMJCR12W3) from the JST and by the JSPS (KAKENHI grant numbers 17H06300 and 17H06299).

AUTHOR CONTRIBUTIONS

H.K. and S.K. conceived the project and designed the experiments. H.K., F.M., and Y.Y. performed the experiments. H.K. and S.U. developed the model and analyzed the data. H.K., Y.Y., and F.M. contributed reagents/materials/analysis tools. H.K. and S.K. wrote the manuscript.

DECLARATION OF INTERESTS

The authors declare no competing interests.

Received: December 14, 2017
Revised: April 6, 2018
Accepted: May 18, 2018
Published: June 27, 2018

REFERENCES

Behar, M., Hao, N., Dohlman, H.G., and Elston, T.C. (2008). Dose-to-duration encoding and signaling beyond saturation in intracellular signaling networks. PLoS Comput. Biol. *4*, e1000197.

Brabant, G., Prank, K., and Schofl, C. (1992). Pulsatile patterns in hormone secretion. Trends Endocrinol. Metab. *3*, 183–190.

Bratusch-Marrain, P.R., Komjati, M., and Waldhausl, W.K. (1986). Efficacy of pulsatile versus continuous insulin administration on hepatic glucose production and glucose utilization in type I diabetic humans. Diabetes *35*, 922–926.

Brown, M.S., and Goldstein, J.L. (2008). Selective versus total insulin resistance: a pathogenic paradox. Cell Metab. *7*, 95–96.

Bruce, D.G., Chisholm, D.J., Storlien, L.H., and Kraegen, E.W. (1988). Physiological importance of deficiency in early prandial insulin secretion in non-insulin-dependent diabetes. Diabetes *37*, 736–744.

Burant, C.F., Treutelaar, M.K., and Buse, M.G. (1986). Diabetes-induced functional and structural changes in insulin receptors from rat skeletal muscle. J. Clin. Invest. *77*, 260–270.

Davies, B., and Morris, T. (1993). Physiological parameters in laboratory animals and humans. Pharm. Res. *10*, 1093–1095.

Dolmetsch, R.E., Lewis, R.S., Goodnow, C.C., and Healy, J.I. (1997). Differential activation of transcription factors induced by Ca2+ response amplitude and duration. Nature *386*, 855–858.

Filippi, S., Barnes, C.P., Kirk, P.D.W., Kudo, T., Kunida, K., McMahon, S.S., Tsuchiya, T., Wada, T., Kuroda, S., and Stumpf, M.P.H. (2016). Robustness of MEK-ERK dynamics and origins of cell-to-cell variability in MAPK signaling. Cell Rep. *15*, 2524–2535.

Grubert, J.M., Lautz, M., Lacy, D.B., Moore, M.C., Farmer, B., Penaloza, A., Cherrington, A.D., and McGuinness, O.P. (2005). Impact of continuous and pulsatile insulin delivery on net hepatic glucose uptake. Am. J. Physiol. Endocrinol. Metab. *289*, E232–E240.

Hoffmann, A., Levchenko, A., Scott, M.L., and Baltimore, D. (2002). The IkappaB-NF-kappaB signaling module: temporal control and selective gene activation. Science *298*, 1241–1245.

Housden, B.E., and Perrimon, N. (2014). Spatial and temporal organization of signaling pathways. Trends Biochem. Sci. *39*, 457–464.

Humphrey, S.J., Azimifar, S.B., and Mann, M. (2015). High-throughput phosphoproteomics reveals in vivo insulin signaling dynamics. Nat. Biotechnol. *33*, 990–995.

Humphrey, S.J., Yang, G., Yang, P., Fazakerley, D.J., Stockli, J., Yang, J.Y., and James, D.E. (2013). Dynamic adipocyte phosphoproteome reveals that Akt directly regulates mTORC2. Cell Metab. *17*, 1009–1020.

Isaksson, O.G.P., Eden, S., and Jansson, J.-O. (1985). Mode of action of pituitary growth hormone on target cells. Annu. Rev. Physiol. *47*, 483–499.

Jaspan, J.B., Lever, E., Polonsky, K.S., and Van Cauter, E. (1986). In vivo pulsatility of pancreatic islet peptides. Am. J. Physiol. *251*, E215–E226.

Koopmans, S.J., Sips, H.C.M., Krans, H.M.J., and Radder, J.K. (1996). Pulsatile intravenous insulin replacement in streptozotocin diabetic rats is more efficient than continuous delivery: effects on glycaemic control, insulin-mediated glucose metabolism and lipolysis. Diabetologia *39*, 391–400.

Kubota, H., Noguchi, R., Toyoshima, Y., Ozaki, Y., Uda, S., Watanabe, K., Ogawa, W., and Kuroda, S. (2012). Temporal coding of insulin action through multiplexing of the AKT pathway. Mol. Cell *46*, 820–832.

Kubota, T., Kubota, N., and Kadowaki, T. (2017). Imbalanced insulin actions in obesity and type 2 diabetes: key mouse models of insulin signaling pathway. Cell Metab. *25*, 797–810.

Lindsay, J.R., McKillop, A.M., Mooney, M.H., Flatt, P.R., Bell, P.M., and O'Harte, F.P. (2003). Meal-induced 24-hour profile of circulating glycated

insulin in type 2 diabetic subjects measured by a novel radioimmunoassay. Metabolism *52*, 631–635.

Noguchi, R., Kubota, H., Yugi, K., Toyoshima, Y., Komori, Y., Soga, T., and Kuroda, S. (2013). The selective control of glycolysis, gluconeogenesis and glycogenesis by temporal insulin patterns. Mol. Syst. Biol. *9*, 664.

O'Meara, N.M. (1993). Analytical problems in detecting rapid insulin secretory pulses in normal humans. Am. J. Physiol. *264*, E231–E238.

O'Rahilly, S., Turner, R.C., and Matthews, D.R. (1988). Impaired pulsatile secretion of insulin in relatives of patients with non-insulin-dependent diabetes. N. Engl. J. Med. *318*, 1225–1230.

Okamoto, Y., Ogawa, W., Nishizawa, A., Inoue, H., Teshigawara, K., Kinoshita, S., Matsuki, Y., Watanabe, E., Hiramatsu, R., Sakaue, H., et al. (2007). Restoration of glucokinase expression in the liver normalizes postprandial glucose disposal in mice with hepatic deficiency of PDK1. Diabetes *56*, 1000–1009.

Paolisso, G., Sgambato, S., Gentile, S., Memoli, P., Giugliano, D., Varricchio, M., and D'Onofrio, F. (1988). Advantageous metabolic effects of pulsatile insulin delivery in noninsulin-dependent diabetic patients. J. Clin. Endocrinol. Metab. *67*, 1005–1010.

Perry, R.J., Camporez, J.P., Kursawe, R., Titchenell, P.M., Zhang, D., Perry, C.J., Jurczak, M.J., Abudukadier, A., Han, M.S., Zhang, X.M., et al. (2015). Hepatic acetyl CoA links adipose tissue inflammation to hepatic insulin resistance and type 2 diabetes. Cell *160*, 745–758.

Polonsky, K.S. (1988). Twenty-four-hour profiles and pulsatile patterns of insulin secretion in normal and obese subjects. J. Clin. Invest. *81*, 442–448.

Pratley, R.E., and Weyer, C. (2001). The role of impaired early insulin secretion in the pathogenesis of type II diabetes mellitus. Diabetologia *44*, 929–945.

Prato, S.D. (2003). Loss of early insulin secretion leads to postprandial hyperglycaemia. Diabetologia *46*, M2–M8.

Purvis, J.E., and Lahav, G. (2013). Encoding and decoding cellular information through signaling dynamics. Cell *152*, 945–956.

Raue, A., Kreutz, C., Maiwald, T., Klingmuller, U., and Timmer, J. (2011). Addressing parameter identifiability by model-based experimentation. IET Syst. Biol. *5*, 120–130.

Sano, T., Kawata, K., Ohno, S., Yugi, K., Kakuda, H., Kubota, H., Uda, S., Fujii, M., Kunida, K., Hoshino, D., et al. (2016). Selective control of up-regulated and down-regulated genes by temporal patterns and doses of insulin. Sci. Signal. *9*, ra112.

Sasagawa, S., Ozaki, Y.-i., Fujita, K., and Kuroda, S. (2005). Prediction and validation of the distinct dynamics of transient and sustained ERK activation. Nat. Cell Biol. *7*, 365–373.

Shah, O.J., Wang, Z., and Hunter, T. (2004). Inappropriate activation of the TSC/Rheb/mTOR/S6K cassette induces IRS1/2 depletion, insulin resistance, and cell survival deficiencies. Curr. Biol. *14*, 1650–1656.

Song, S.H. (2000). Direct measurement of pulsatile insulin secretion from the portal vein in human subjects. J. Clin. Endocrinol. Metab. *85*, 4491–4499.

Titchenell, P.M., Quinn, W.J., Lu, M., Chu, Q., Lu, W., Li, C., Chen, H., Monks, B.R., Chen, J., Rabinowitz, J.D., et al. (2016). Direct hepatocyte insulin signaling is required for lipogenesis but is dispensable for the suppression of glucose production. Cell Metab. *23*, 1154–1166.

Uda, S., Saito, T.H., Kudo, T., Kokaji, T., Tsuchiya, T., Kubota, H., Komori, Y., Ozaki, Y.-i., and Kuroda, S. (2013). Robustness and compensation of information transmission of signaling pathways. Science *341*, 558–561.

Urakubo, H., Honda, M., Tanaka, K., and Kuroda, S. (2009). Experimental and computational aspects of signaling mechanisms of spike-timing-dependent plasticity. HFSP J. *3*, 240–254.

Vaudry, D., Stork, P.J.S., Lazarovici, P., and Eiden, L.E. (2002). Signaling pathways for PC12 cell differentiation: making the right connections. Science *296*, 1648–1649.

Wang, Y., Viscarra, J., Kim, S.J., and Sul, H.S. (2015). Transcriptional regulation of hepatic lipogenesis. Nat. Rev. Mol. Cell Biol. *16*, 678–689.

Whiteman, E.L., Cho, H., and Birnbaum, M.J. (2002). Role of Akt/protein kinase B in metabolism. Trends Endocrinol. Metab. *13*, 444–451.

Yugi, K., Kubota, H., Toyoshima, Y., Noguchi, R., Kawata, K., Komori, Y., Uda, S., Kunida, K., Tomizawa, Y., Funato, Y., et al. (2014). Reconstruction of insulin signal flow from phosphoproteome and metabolome data. Cell Rep. *8*, 1171–1183.

Please cite this article in press as: Kubota et al., *In Vivo* Decoding Mechanisms of the Temporal Patterns of Blood Insulin by the Insulin-AKT Pathway in the Liver, Cell Systems (2018), https://doi.org/10.1016/j.cels.2018.05.013

STAR★METHODS

KEY RESOURCES TABLE

REAGENT or RESOURCE	SOURCE	IDENTIFIER
Antibodies		
Rabbit Monoclonal anti-Insulin Receptor beta	Cell Signaling Technology	Cat#: 3025 RRID: AB_2280448
Rabbit Monoclonal anti-pTyr1150/1151 Insulin Receptor beta	Cell Signaling Technology	Cat#: 3024 RRID: AB_331253
Rabbit Monoclonal anti-AKT (pan)	Cell Signaling Technology	Cat#: 4691 RRID: AB_915783
Rabbit Monoclonal anti-pThr308 Akt	Cell Signaling Technology	Cat#: 2965 RRID: AB_2255933
Rabbit Monoclonal anti-pSer473 Akt	Cell Signaling Technology	Cat#: 4058 RRID: AB_331168
Rabbit Monoclonal anti-p70 S6 Kinase	Cell Signaling Technology	Cat#: 2708 RRID: AB_390722
Rabbit Monoclonal anti-pThr389 p70 S6 Kinase	Cell Signaling Technology	Cat#: 9234 RRID: AB_2269803
Rabbit Monoclonal anti-GSK-3β	Cell Signaling Technology	Cat#: 12456 RRID: AB_2636978
Rabbit Monoclonal anti-pSer9 GSK-3β	Cell Signaling Technology	Cat#: 9323 RRID: AB_2115201
Rabbit Monoclonal anti-FoxO1	Cell Signaling Technology	Cat#: 2880 RRID: AB_2106495
Rabbit Polyclonal anti-pSer256 FoxO1	Cell Signaling Technology	Cat#: 9461 RRID: AB_329831
Chemicals, Peptides, and Recombinant Proteins		
Insulin	SIGMA	Cat#: 12643
somatostatin	Bachem AG	H-1490
isoflurane	Pfizer	N/A
Critical Commercial Assays		
insulin ELISA kit	Shibayagi	AKRIN-010T
BCA Protein Assay Kit	Thermo	Cat: 23227
SuperSignal West Dura Extended Duration Substrate	Thermo	Cat: 34075
RNAeasy Mini,	Qiagen	Cat: 74106
QuantiTect Reverse Transcription Kit	Qiagen	Cat: 205313
KAPA SYBR FAST Universal qPCR Kit	KAPA Biosystems	Cat: KK4802
Experimental Models: Cell Lines		
Male SD rat	Japan SLC	N/A
Oligonucleotides		
Primers for qRT-PCR, see Text	This paper	N/A
Software and Algorithms		
MATLAB R2016a	MathWorks	https://www.mathworks.com/
In Vivo Insulin Model (MATLAB file)	This paper	N/A
TotalLab TL120	Nonlinear Dynamics	N/A
Other		
Fusion Solo S	Vilber Lourmat	N/A
LightCycler 96	Roche	N/A

CONTACTS FOR REAGENT AND RESOURCE SHARING

Further information and requests for reagents and resources should be directed to and will be fulfilled by the Lead Contact, Hiroyuki Kubota (kubota@bioreg.kyushu-u.ac.jp).

EXPERIMENTAL MODEL AND SUBJECT DETAILS

Animal Procedures

The institutional animal care and use committee at Kyushu University approved all rat studies. Male SD rats (10 weeks old) were purchased from Japan SLC. We conducted all rat experiments just after purchasing. After overnight fasting, the rats were anesthetized using isoflurane. To suppress endogenous insulin secretion, somatostatin was administered through the jugular vein (3 μg/kg/min). Insulin was administered through the mesenteric vein at the indicated dose (7 μl/kg/min), maintaining the blood glucose concentration at a constant level using 50% glucose (150 mg/dl). Blood was sampled at the indicated time points via the tail vein, and blood insulin concentrations were measured using a rat insulin enzyme-linked immunosorbent assay kit (ELISA kit; Shibayagi, #AKRIN-010T). At the indicated time points, the rats were sacrificed and their livers were immediately frozen by liquid nitrogen. We obtained one data point from one animal.

METHOD DETAILS

Western Blotting

Frozen livers were crushed with dry ice, including protease inhibitors (Thermo, #78429) and phosphatase inhibitors (Nacalai, #07574-61). The samples were dispensed into several tubes. After sublimation of dry ice at −80°C, 1 ml of MeOH was added into one of the tubes. The tube was mixed well and 400 μl of water was added. After centrifugation at 4,600 × *g* for 15 minutes, the pellet was washed with 400 μl of $CHCl_3$ and 600 μl of MeOH. After centrifuging again (4,600 × *g* for 15 minutes), the pellet was suspended by lysis buffer (3% SDS, 50 mM Tris pH 6.8). The protein concentration was measured using a BCA Protein Assay Kit (Thermo, #23227), and adjusted to 1 mg/ml using sample buffer (final concentration: 3% SDS, 50 mM Tris pH 6.8, 10% glycerol 5% 2-mercaptoethanol). The samples (5 μl/lane) were subjected to SDS-PAGE. The resolved proteins were transferred to polyvinylidene difluoride membranes (Millipore, #IPVH00010) and probed with specific antibodies (Antibodies against IR beta [#3025], pIR beta [#3024], AKT [#4691], pAKT [Thr^{308}, #2965], S6K [#2708], pS6K [Thr^{389}, #9234], GSK3β [#12456], pGSK3β [Ser^{9}, #9323], FoxO1 [#2880], pFoxO1 [Ser^{256}, #9461]: purchased from Cell Signaling Technology) and secondary antibody against Rabbit IgG (SIGMA, #A6154-1ML). Thr308 and Ser473 are phosphorylated by PDK1 and mTORC2, respectively. Since PDK1 is located between IR and AKT, we assumed the phosphorylation at Thr308 was better than that at Ser473 for modeling in this study. Also, we confirmed that the phosphorylations at Thr308 and Ser473 showed similar time courses (Figure S1D). The signals were visualized using SuperSignal West Dura Extended Duration Substrate (Thermo, #34075) and detected using a Fusion Solo S (Vilber Lourmat). The intensities of bands were quantified using TotalLab TL120 analysis software (Nonlinear Dynamics).

To compare the intensity among the membranes, we chose six samples from two time points of each doses from different 3 membranes whose phosphorylation intensities were highest. Then, we compared these 18 samples on the same membrane using antibodies against 8 molecules (IR, pIR, AKT, pAKT, GSK3β, pGSK3β, S6K and pS6K) by western blotting analysis. We calculated "correction coefficient" among the membranes and corrected the intensity among the three doses (membranes). The phosphorylation levels were normalized by the amount of each total protein. We set the maximal peak intensity of each phosphorylation level to 1, so that the signal intensities in different experiments were comparable among figures.

RNA Isolation and Quantitative Real-Time Reverse Transcription PCR (qRT-PCR) Analysis

Buffer RLT (RNAeasy Mini, Qiagen, #74106) was added directly into the tubes containing the liver samples described above (western blotting section), so that the samples for western blotting and RT-PCR were derived from the same sample. We isolated total RNAs according to the kit's instruction. RNA samples were reverse transcribed using a QuantiTect Reverse Transcription Kit (Qiagen, #205313). qRT-PCR was performed using a KAPA SYBR FAST Universal qPCR Kit (KAPA Biosystems, #KK4802) and specific primers (*G6Pase*: forward [5′-CTCACTTTCCCCATCAGGTG-3′] and reverse [5′-GAAAGTTTCAGCCACAGCAA-3′], *36B4*: forward [5′-GATGCCCAGGGAAGACAG-3′] and reverse [5′-CACAATGAAGCATTTTGGGTAG-3′]) using LightCycler 96 (Roche). Quantification of *G6Pase* was performed by ΔΔCt method using *36B4* as an internal standard.

Simulation and Parameter Estimation

We developed the blood-insulin model and the insulin pathway model, and performed simulation and parameter estimations using Matlab (version R2016a, Math Works). Model structures, reactions, parameters, and differential equations are described in Figure S3. Parameter estimation was performed as described previously (Kubota et al., 2012). In short, the parameters of the model were estimated using experimental data in Figures 1D, 2C, and 2F according to two methods in series. First, a meta-evolutionary programming method was used to approach the neighborhood of the local minimum. Second, the Nelder-Mead method was used to reach the local minimum. Using these methods, the parameters were estimated to minimize the sum of the square residuals between the experimental data and the model trajectories.

Please cite this article in press as: Kubota et al., *In Vivo* Decoding Mechanisms of the Temporal Patterns of Blood Insulin by the Insulin-AKT Pathway in the Liver, Cell Systems (2018), https://doi.org/10.1016/j.cels.2018.05.013

Administered insulin concentration at the portal vein was calculated according to the injection rate (7 μl/kg/min) and the blood flow rate at the rat portal vein (39.2 ml/kg/min) (Davies and Morris, 1993). The blood insulin concentration did not reach 0, even if we administered somatostatin for 3 hours; therefore, the basal insulin concentration was defined in the model (Figure S3B).

The Insulin-AKT pathway model was developed according to our previous insulin-dependent AKT pathway model (Kubota et al., 2012), except for three major changes as follows (Figure S3C). The first is the regulation of IR, which was not incorporated in our previous model. The second one is the regulation of insulin receptor substrate proteins (IRSs). It is reported that protein levels of IRSs decrease in response to long insulin exposure (Shah et al., 2004). However, under our experimental condition within 2 hours, the amount of IRS1 did not decrease significantly. Therefore, we did not consider degradation in our current model. The last one is the regulation of GSK3ß. In our previous model, the phosphorylation level of GSK3ß was only regulated by pAKT. First, we developed the GSK3ß model according to our previous structure; however, the model could not sufficiently reproduce the experimental time courses of GSK3ß (Figure S3D). Therefore, we assumed constant phosphorylation by molecule Y which did not depend on insulin stimulation and developed the model (Figure S3C). The later model successfully reproduced the experimental time courses of GSK3ß (Figure S3D). Then, model fitness was compared using the Akaike Information Criterion (AIC). The AIC of the model with regulation Y was smaller than that without regulation Y, indicating that the model with regulation Y was more reliable than that without. Therefore, we chose the model with regulation Y in the Insulin-AKT pathway model. The number of parameters for the Insulin-AKT pathway model was large; therefore, we could not efficiently estimate all parameters at once. Therefore, we separated the model into small modules (Figure S3C) and estimated the parameters of the model depending on the modules. Then, all parameters were estimated again by limiting the upper and lower limits of the parameters to 100 and 1/100 times that of the estimated parameter, respectively. The fitting error may be larger by this restriction. However, the computational costs greatly decrease. We need to examine this issue in detail (Raue et al., 2011). However, more importantly, our model reproduced the dynamics enough to reveal the mechanisms.

Definition of IRI, SI and PRI

IRI is defined as

$$IRI = \frac{|Intensity_{25-75}|}{time_{25-75}}$$

where $Intensity_{25\text{-}75}$ and $time_{25\text{-}75}$ indicate the changes of intensity and time in molecules from 25 to 75% of the maximal response, respectively.

SI is defined as

$$SI = |correlation|$$

where correlation indicates the correlations between time course of insulin and that of each molecule.

PRI is defined as

$$PRI = \frac{Peak\_\sin - Peak\_adm}{Peak\_\max - Peak\_adm}$$

where Peak_sin, Peak_adm, and Peak_max indicate the peak of Stim_sin, Stim_adm, and Stim_max respectively. Stim_sin indicates the time course of the molecules stimulated by the indicated insulin sinusoidal waves with different frequencies. Stim_adm indicates one of two control stimulations whose amount of administered insulin per time was the same as that of the Stim_sin. Stim_max indicates the other control stimulation whose maximal amplitude was the same as that of the Stim_sin.

Note that all the indexes of *G6Pase* in this study were determined based on the absolute difference from the basal level.

DATA AND SOFTWARE AVAILABILITY

Matlab code of the model is shown.